Atherosclerosis 322 (2021) 51–60

Contents lists available at ScienceDirect

Atherosclerosis

journal homepage: www.elsevier.com/locate/atherosclerosis

Impact of myeloid *RIPK1* gene deletion on atherogenesis in ApoE-deficient mice

Isabelle Coornaert [a], Pauline Puylaert [a], Giullia Marcasolli [a], Mandy O.J. Grootaert [a,1], Peter Vandenabeele [b,c,d], Guido R.Y. De Meyer [a], Wim Martinet [a,*]

[a] Laboratory of Physiopharmacology, Department of Pharmaceutical Sciences, University of Antwerp, Universiteitsplein 1, B-2610, Antwerp, Belgium
[b] VIB Center for Inflammation Research, Technologiepark 927, B-9052, Ghent, Belgium
[c] Department of Biomedical Molecular Biology (DBMB), Ghent University, B-9052, Ghent, Belgium
[d] Methusalem Program CEDAR-IC, Ghent University, B-9052, Ghent, Belgium

ARTICLE INFO

Keywords:
Atherosclerosis
Necroptosis
RIPK1
Apoptosis

ABSTRACT

Background and aims: Targeting macrophage death is a promising strategy for stabilizing atherosclerotic plaques. Recently, necroptosis was identified as a form of regulated necrosis in atherosclerosis. Receptor-interacting serine/threonine-protein kinase (RIPK)1 is an upstream regulator of RIPK3, which is a crucial kinase for necroptosis induction. We aimed to investigate the impact of myeloid-specific *RIPK1* gene deletion on atherogenesis.
Methods: *RIPK1*$^{F/F}$*LysM-Cre*$^{+}$*ApoE*$^{-/-}$ and *RIPK1*$^{+/+}$*LysM-Cre*$^{+}$*ApoE*$^{-/-}$ mice were fed a western-type diet (WD) for 16 or 24 weeks to induce plaque formation.
Results: After 16 weeks WD, plaque area and percentage necrosis in *RIPK1*$^{F/F}$*LysM-Cre*$^{+}$*ApoE*$^{-/-}$ mice were significantly decreased as compared to plaques of *RIPK1*$^{+/+}$*LysM-Cre*$^{+}$*ApoE*$^{-/-}$ mice. Moreover, plaques of *RIPK1*$^{F/F}$*LysM-Cre*$^{+}$*ApoE*$^{-/-}$ mice showed more apoptosis and a decreased macrophage content. After 24 weeks WD, plaque size and percentage necrosis were no longer different between the two groups. Free apoptotic cells strongly accumulated in plaques of *RIPK1*$^{F/F}$*LysM-Cre*$^{+}$*ApoE*$^{-/-}$ mice. In addition to apoptosis, necroptosis was upregulated in plaques of *RIPK1*$^{F/F}$*LysM-Cre*$^{+}$*ApoE*$^{-/-}$ mice. *In vitro,* TNF-α triggered apoptosis in *RIPK1*$^{F/F}$*LysM-Cre*$^{+}$*ApoE*$^{-/-}$, but not in *RIPK1*$^{+/+}$*LysM-Cre*$^{+}$*ApoE*$^{-/-}$ macrophages. Moreover, *RIPK1*$^{F/F}$*LysM-Cre*$^{+}$*ApoE*$^{-/-}$ macrophages were not protected against RIPK3-dependent necroptosis.
Conclusions: The impact of myeloid *RIPK1* gene deletion depends on the stage of atherogenesis. At 16 weeks WD, myeloid *RIPK1* gene deletion resulted in increased apoptosis, thereby slowing down plaque progression. However, despite decreased macrophage content, plaque and necrotic core size were no longer reduced after 24 weeks of WD, most likely due to the accumulation of free apoptotic and necroptotic cells.

1. Introduction

Atherosclerosis is a chronic inflammatory disease characterized by the accumulation of atherosclerotic plaques in medium- and large-sized arteries [1]. During plaque development, macrophages and vascular smooth muscle cells (VSMCs) undergo necrosis and release their cytoplasmic content in the plaque, which initiates the formation of a central necrotic core. Different stimuli such as enhanced oxidative stress, depletion of cellular ATP and increased levels of intracellular calcium trigger necrosis in atherosclerosis [2,3]. Moreover, because the phagocytic clearance of apoptotic cells (AC) by macrophages is impaired in advanced lesions [4], AC accumulate and undergo secondary necrosis. Necrotic cells enhance plaque inflammation by releasing pro-inflammatory cytokines and damage-associated molecular patterns (DAMPs) [5]. Interestingly, lipids in the form of cholesterol esters soften the necrotic core. A soft core makes the plaque more vulnerable because it is not able to bear the imposed circumferential stress [6]. The mechanical forces are redistributed to the fibrous cap and may trigger plaque rupture. In approximately two-thirds of ruptured plaques, the necrotic core occupies more than 25% of the plaque area [2].

* Corresponding author.
E-mail address: Wim.Martinet@uantwerpen.be (W. Martinet).
[1] Present address: Division of Cardiovascular Medicine, Department of Medicine, University of Cambridge, Box 110, Addenbrooke's Centre for Clinical Investigation, Addenbrooke's Hospital, Cambridge CV2 0QQ, UK.

https://doi.org/10.1016/j.atherosclerosis.2021.02.021
Received 19 August 2020; Received in revised form 23 December 2020; Accepted 19 February 2021
Available online 24 February 2021

For many years, necrosis has been considered as an uncontrolled way for a cell to die, and therefore has not been extensively investigated in atherosclerosis. However, besides accidental necrosis, necrotic death can also occur in a regulated fashion, termed regulated necrosis. Different types of regulated necrosis such as necroptosis, pyroptosis and parthanatos have been identified in advanced plaques [3]. Hitherto, necroptosis induced by TNF-α is the best-investigated form of regulated necrosis. Upon activation of the TNF receptor, a series of auto- and transphosphorylation events of receptor-interacting protein kinase (RIPK)1 and RIPK3 activate necroptosis signaling [7]. Activated RIPK3 phosphorylates mixed lineage kinase domain like pseudokinase (MLKL), which in turn punctures the plasma membrane [8,9]. Recent studies revealed elevated expression levels of RIPK1, RIPK3 and phosphorylated MLKL in human plaques associated with necrotic core formation and an unstable plaque phenotype, yet which cells are mostly expressing these necroptosis markers was not demonstrated [10,11]. In mice, *RIPK3* gene deletion in *LDLr*$^{-/-}$ mice reduces plaque size in advanced atherosclerotic lesions [12]. Moreover, treatment of atherosclerotic *ApoE*$^{-/-}$ mice with Nec-1s, which is a small molecule necroptosis inhibitor that inhibits the kinase activity of RIPK1, reduces atherosclerotic plaque size and promotes a stable plaque phenotype [11]. More recently, it has been demonstrated that MLKL loss reduces necrotic core size and cell death in *ApoE*$^{-/-}$ mice, albeit without changing plaque size [13]. Overall, these findings highlight the major impact of RIPK1/3-mediated necroptosis in advanced atherosclerosis.

Importantly, potential beneficial effects of *RIPK1* gene deletion have not yet been studied in atherosclerosis, most likely because a full body knockout of RIPK1 causes perinatal lethality [14]. Besides its role in necroptosis (and unlike RIPK3), RIPK1 plays an important role in caspase-dependent apoptosis and cell survival via NF-κB-mediated gene induction [15,16]. The kinase activity of RIPK1 is crucial for promoting cell death, but it is not essential for its pro-survival function [17]. The mechanisms by which RIPK1 switches from a pro-survival protein to a pro-death protein remain largely unknown, but likely depend on the ubiquitination and phosphorylation state of RIPK1 [18–22]. In the present study, we report that RIPK1 is mainly expressed in macrophage-rich regions of human plaques. Accordingly, we investigated the impact of myeloid *RIPK1* gene deletion on atherogenesis and necrotic core formation by crossbreeding myeloid-specific RIPK1 knockout (*RIPK1*$^{F/F}$*LysM-Cre*$^{+}$) mice with ApoE knockout (*ApoE*$^{-/-}$) mice.

2. Materials and methods

2.1. Human atherosclerotic plaques

Human carotid endarterectomy specimens were obtained from patients (71 ± 3 years, 70% men) with a carotid stenosis of >70%. Specimens were fixed in 4% formaldehyde (pH 7.4) within 2 min after surgical removal and paraffin embedded. To identify specific cell types expressing RIPK1, fluorescent double staining using anti-RIPK1 (Novus Biologicals, NB100-56160) and anti-CD68 (DAKO, clone PG-M1) or anti-α-smooth muscle actin (α-SMA; Sigma, A2547) was performed. After mounting tissue samples with VECTASHIELD mounting medium containing 4,6-diamidino-2-phenylindole (DAPI; Vector laboratories, H-1200), images were acquired using a Celena S digital Imaging System (Logos Biosystems).

2.2. Mice

Mice homozygous for the *RIPK1*$^{\text{Flox}}$ allele (*RIPK1*$^{F/F}$ mice) [23] were crossbred with transgenic mice that express Cre recombinase under control of the mouse lysozyme M promoter (*LysM-Cre*$^{+}$ mice, Jackson Laboratory, stock number 004781) to obtain myeloid-specific *RIPK1* knock-out mice. To study the impact of RIPK1-deficient myeloid cells in atherosclerosis, *RIPK1*$^{F/F}$*LysM-Cre*$^{+}$ mice were further crossbred with apolipoprotein E deficient (*ApoE*$^{-/-}$) mice (Jackson Laboratory, stock number 002052). Resulting *RIPK1*$^{F/F}$*LysM-Cre*$^{+}$ *ApoE*$^{-/-}$ mice as well as *RIPK1*$^{+/+}$*LysM-Cre*$^{+}$ *ApoE*$^{-/-}$ controls were fed a western-type diet (WD; C1000 diet supplemented with 20% milkfat and 0.15% cholesterol, #100171, Altromin) starting at the age of 6 weeks to induce plaque formation. The animals were housed in a temperature-controlled room with a 12 h light/dark cycle and had free access to water and food. After 16 weeks or 24 weeks WD, blood samples were collected via the retro-orbital plexus of anesthetized mice (sodium pentobarbital 75 mg/kg, i.p.). Subsequently, mice were sacrificed with sodium pentobarbital (250 mg/kg, i.p.). Blood leukocyte subsets were analyzed by flow cytometry as previously described [24]. Total plasma cholesterol, triglycerides and LDL cholesterol levels were measured on an automated Vista 1500 System (Siemens Healthcare Diagnostics). All experiments were approved by the Ethical Committee of the University of Antwerp.

2.3. Histological analyses

After sacrificing *RIPK1*$^{F/F}$*LysM-Cre*$^{+}$ *ApoE*$^{-/-}$ and *RIPK1*$^{+/+}$*LysM-Cre*$^{+}$ *ApoE*$^{-/-}$ mice, the thoracic aorta, brachiocephalic artery and the aortic root were collected. The thoracic aorta was stained *en face* with Oil Red O to determine plaque burden. The brachiocephalic artery was fixed in 4% formalin for 24 h, dehydrated overnight in 60% isopropanol, and subsequently embedded in paraffin. Serial cross sections of the brachiocephalic artery were prepared for histological analyses. Atherosclerotic plaque size, maximum plaque thickness and necrotic core area (defined as acellular areas with a threshold of 3000 μm^2) were analyzed on haemotoxylin-eosin (H&E) stained sections. Collagen content was analyzed with Sirius red. To stain plaques for myeloperoxidase, sections were incubated for 30 min in 0.05% 3,3-diaminobenzidine (DAB) solution. Macrophages were detected by immunohistochemistry using Mac3 antibodies (BD Pharmingen, 550292). The percentage of VSMCs and maximum fibrous cap thickness was determined on α-SMC actin (Sigma, A2547) stained sections. Apoptosis was evaluated by terminal deoxynucleotidyl transferase dUTP nick end labeling (TUNEL; S7101, Millipore). Cleavage of caspase-3 was detected by immunohistochemistry using cleaved caspase-3 (Asp175) antibodies (Cell Signaling Technology, #9661). The aortic root was embedded in Neg-50 (Thermo Scientific) and snap-frozen in liquid nitrogen. To study *in situ* efferocytosis in atherosclerotic plaques located in the aortic root, cryosections were double stained with rat anti-CD68 (AbD Serotec, MCA1957GA) and TUNEL reagents (Roche, 11684795910). After mounting tissue samples with VECTASHIELD mounting medium containing 4,6-diamidino-2-phenylindole (DAPI; Vector laboratories, H-1200), images were acquired using a Celena S digital Imaging System (Logos Biosystems). All other images were acquired with Universal Grab 6.1 software using an Olympus BX40 light microscope and quantified with Image J software (National Institutes of Health).

2.4. Cell culture

Bone marrow-derived macrophages (BMDMs) were isolated by flushing bone marrow of the femur of mice. Cells were cultured for 7 days in RPMI 1640 medium supplemented with Glutamax (Gibco Life Technology), supplemented with 15% L929-cell conditioned medium (LCCM) containing monocyte colony stimulating factor (M-CSF). VSMCs were isolated as previously described [25,26]. BMDMs were treated with mTNF-α (Abcam), lipopolysaccharide (LPS, Sigma-Aldrich) and zVAD-fmk (Enzo Life Science, ALX-260-020-M001) as indicated in the figure legends. Cell death was evaluated by labeling cells with 1 μg/mL propidium iodide (PI, Molecular Probes) and 10 μg/mL Hoechst (Life Technologies), followed by visualization of PI/Hoechst-labeled cells using a Celena S digital Imaging System (Logos Biosystems).

2.5. In vitro phagocytosis assay

U937 monocytes (American Type Culture Collection) were grown in RPMI 1640 medium supplemented with Glutamax. To generate AC, U937 monocytes were treated with etoposide (Abcam, ab120227). Subsequently, AC were washed to remove non-incorporated etoposide and labeled with 10 μM CellTracker Green CMFDA (Molecular Probes). Phagocytosis of AC was studied by flow cytometry as described [27].

2.6. Western blotting

Samples were lysed in Laemmli sample buffer (Bio-Rad) containing 5% β-mercaptoethanol (Sigma-Aldrich) and heat-denatured for 5 min in boiling water. They were loaded on Bolt 4–12% Bis-Tris gels (Invitrogen) and after electrophoresis transferred to Immobilon-FL PVDF membranes (Millipore) according to standard procedures. Subsequently, membranes were blocked for 1 h in Odyssey Li-COR blocking buffer. After blocking, membranes were probed overnight at 4 °C with primary antibodies diluted in Odyssey Li-COR blocking buffer followed by 1 h incubation with IRDye-labeled secondary antibodies at room temperature. Membranes were visualized with an Odyssey SA infrared imaging system (Li-COR Biosciences).

The following primary antibodies were used: mouse anti-β-actin (Abcam, Ab8226), mouse anti-RIPK1 (BD Transduction Laboratories, 610459), rabbit anti-phospho-RIPK3 (Abcam, ab195117), rabbit anti-RIPK3 (Sigma-Aldrich, R4277), rabbit anti-MLKL (Abcam, ab172868), rabbit anti-phospho-MLKL (Abcam, ab196436), rabbit anti-cleaved caspase 3 (Cell Signaling Technology, #9661), rabbit anti-phospho–NF–κB p65 (Ser536) (Cell Signaling Technology, #3031), rabbit anti–NF–κB p65 (Cell Signaling Technology, #4764), rabbit anti-IκBα (Cell Signaling Technology, #9242) and rabbit anti-phospho-IκBα (Cell Signaling Technology, #9246). IRDye-labeled secondary antibodies (IgG926-32211 (goat anti-rabbit); IgG926-68070 (goat anti-mouse)) were purchased from Li-COR Biosciences.

2.7. Real time RT-PCR

Total RNA was extracted using the Isolation II RNA mini kit (Bioline, BIO-52073) according to the manufacturer's instructions. After reverse transcription with a Sensifast™ cDNA Synthesis Kit (Bioline, BIO-65054), TaqMan gene expression assays for TNF-α (Mm00443258_m1) and IL-1β (Mm00434228_m1) were performed in triplicate on a Quantstudio 3 PCR system (Applied Biosystems). The parameters for PCR amplification were 50 °C for 2 min, 95 °C for 2 min, followed by 40 cycles of 95 °C for 1 s and 60 °C for 20 s. A TaqMan Fast Advanced Master Mix (Applied Biosystems) was used for each reaction. Relative expression of mRNA was calculated using the comparative threshold cycle method. Normalization was performed using β-actin (Mm00607939_s1) and peptidyl isomerase A (Mm02342430_g1), which were validated as stable housekeeping genes.

2.8. Statistical analyses

Statistical analyses were performed using SPSS software (version 25, SPSS Inc.). All data were expressed as mean ± SEM. Statistical tests are specified in the figure legends. Differences were considered significant at $p < 0.05$.

3. Results

3.1. RIPK1 is highly expressed in macrophages of human carotid plaques

To identify which cells in atherosclerotic plaques express RIPK1, human carotid plaques were immuno-stained for RIPK1 in combination with immunodetection of CD68 (monocytes/macrophages) and α-smooth muscle actin (VSMCs). RIPK1 showed co-localization with CD68-positive cells (Fig. 1A and C) but could not be detected in α-smooth muscle actin-positive regions (Fig. 1B and C), suggesting that RIPK1 was mainly expressed in plaque macrophages. To further investigate the role of myeloid RIPK1 expression in atherosclerosis, we generated *RIPK1*$^{F/F}$*LysM-Cre*$^{+}$ mice and *RIPK1*$^{+/+}$*LysM-Cre*$^{+}$ controls. Both mouse strains were further crossbred on an *ApoE*$^{-/-}$ background. BMDM and aortic VSMCs were isolated from the resulting *RIPK1*$^{+/+}$*LysM-Cre*$^{+}$ *ApoE*$^{-/-}$ and *RIPK1*$^{F/F}$*LysM-Cre*$^{+}$ *ApoE*$^{-/-}$ mice to validate macrophage RIPK1 deficiency. RIPK1 was completely absent in *RIPK1*$^{F/F}$*LysM-Cre*$^{+}$ *ApoE*$^{-/-}$ BMDM, though still present in *RIPK1*$^{F/F}$*LysM-Cre*$^{+}$ *ApoE*$^{-/-}$ VSMCs. In *RIPK1*$^{+/+}$*LysM-Cre*$^{+}$ *ApoE*$^{-/-}$ mice, expression levels of RIPK1 were substantially higher (approximately 3-fold) in BMDM as compared to VSMCs (Fig. 1D).

3.2. Myeloid RIPK1 deficiency reduces total plaque size and percentage necrosis in ApoE$^{-/-}$ mice after 16 weeks western-type diet, but not after 24 weeks

RIPK1$^{F/F}$*LysM-Cre*$^{+}$ *ApoE*$^{-/-}$ and *RIPK1*$^{+/+}$*LysM-Cre*$^{+}$ *ApoE*$^{-/-}$ mice were fed a western-type diet (WD) for 16 weeks. After 16 weeks WD, body weight (29 ± 1 *vs.* 30 ± 1 g; independent samples *t*-test, $p > 0.05$) did not change between *RIPK1*$^{F/F}$*LysM-Cre*$^{+}$ *ApoE*$^{-/-}$ and *RIPK1*$^{+/+}$*LysM-Cre*$^{+}$ *ApoE*$^{-/-}$ mice. Plasma analyses did not reveal any differences in the levels of total cholesterol (825 ± 59 *vs.* 964 ± 108 mg/dL; independent samples *t*-test, $p > 0.05$) and triglycerides (148 ± 20 *vs.* 141 ± 28 mg/dL; independent samples *t*-test, $p > 0.05$) between *RIPK1*$^{F/F}$*LysM-Cre*$^{+}$ *ApoE*$^{-/-}$ mice and *RIPK1*$^{+/+}$*LysM-Cre*$^{+}$ *ApoE*$^{-/-}$ controls. Furthermore, the relative percentage of circulating leukocyte subsets was not affected by macrophage-specific *RIPK1* gene deletion (Supplementary Fig. 1). *En face* oil red O stainings showed a significant decrease of lipid deposition in the thoracic aorta of *RIPK1*$^{F/F}$*LysM-Cre*$^{+}$ *ApoE*$^{-/-}$ mice after 16 weeks WD (Fig. 2A). Analysis of H&E-stained cross-sections of the brachiocephalic artery demonstrated that the plaque area (72 ± 7 *vs.* 150 ± 12 × 10^3 μm^2; independent samples *t*-test, $p < 0.001$) and percentage necrosis in *RIPK1*$^{F/F}$*LysM-Cre*$^{+}$ *ApoE*$^{-/-}$ mice was significantly decreased as compared to *RIPK1*$^{+/+}$*LysM-Cre*$^{+}$ *ApoE*$^{-/-}$ mice (Fig. 2B). The ratio maximum fibrous cap thickness/maximum plaque thickness tended to be smaller in *RIPK1*$^{F/F}$*LysM-Cre*$^{+}$ *ApoE*$^{-/-}$ mice (Supplementary Fig. 2B), but this difference was not statistically significant. Conversely, plaques of *RIPK1*$^{F/F}$*LysM-Cre*$^{+}$ *ApoE*$^{-/-}$ mice showed increased TUNEL positivity as compared to *RIPK1*$^{+/+}$*LysM-Cre*$^{+}$ *ApoE*$^{-/-}$ mice (Fig. 2C), albeit changes in immunoreactivity for cleaved caspase-3 were not detected (0.64 ± 0.19 *vs.* 0.47 ± 0.09%; independent samples *t*-test, $p = 0.416$). Further analysis of the cellular composition of plaques revealed that the macrophage content decreased significantly in plaques of *RIPK1*$^{F/F}$*LysM-Cre*$^{+}$ *ApoE*$^{-/-}$ mice (Fig. 2D). However, the amount of VSMCs was not different in *RIPK1*$^{F/F}$*LysM-Cre*$^{+}$ *ApoE*$^{-/-}$ and *RIPK1*$^{+/+}$*LysM-Cre*$^{+}$ *ApoE*$^{-/-}$ mice (Supplementary Fig. 2A), nor was the total collagen content changed (Supplementary Fig. 2B). The majority of plaques in both groups was negative for myeloperoxidase (data not shown), which is an enzyme that is most abundantly expressed in neutrophils.

After 24 weeks WD, total plasma cholesterol (819 ± 73 *vs.* 558 ± 46 mg/dL; independent samples *t*-test, $p < 0.01$) was significantly increased in *RIPK1*$^{F/F}$ *LysMCre*$^{+}$ *ApoE*$^{-/-}$ mice as compared to *RIPK1*$^{+/+}$ *LysMCre*$^{+}$ *ApoE*$^{-/-}$ mice. Triglyceride levels (94 ± 13 *vs.* 81 ± 13 mg/dL; independent samples *t*-test, $p > 0.05$) and body weight (26 ± 1 *vs.* 24 ± 2 g, independent samples *t*-test, $p > 0.05$) were not different between both groups. In contrast to 16 weeks WD, lipid deposition (Fig. 3A), plaque size (126 ± 17 *vs.* 148 ± 19 × 10^3 μm^2; independent samples *t*-test, $p > 0.05$) and percentage necrosis were similar between *RIPK1*$^{+/+}$*LysM-Cre*$^{+}$ *ApoE*$^{-/-}$ and *RIPK1*$^{F/F}$*LysM-Cre*$^{+}$ *ApoE*$^{-/-}$ mice, respectively (Fig. 3B), even though the number of TUNEL positive cells was still elevated in plaques of *RIPK1*$^{F/F}$ *ApoE*$^{-/-}$ mice (Fig. 3C). The ratio maximum fibrous cap thickness/maximum plaque thickness was significantly decreased in *RIPK1*$^{+/+}$*LysM-Cre*$^{+}$ *ApoE*$^{-/-}$ mice as

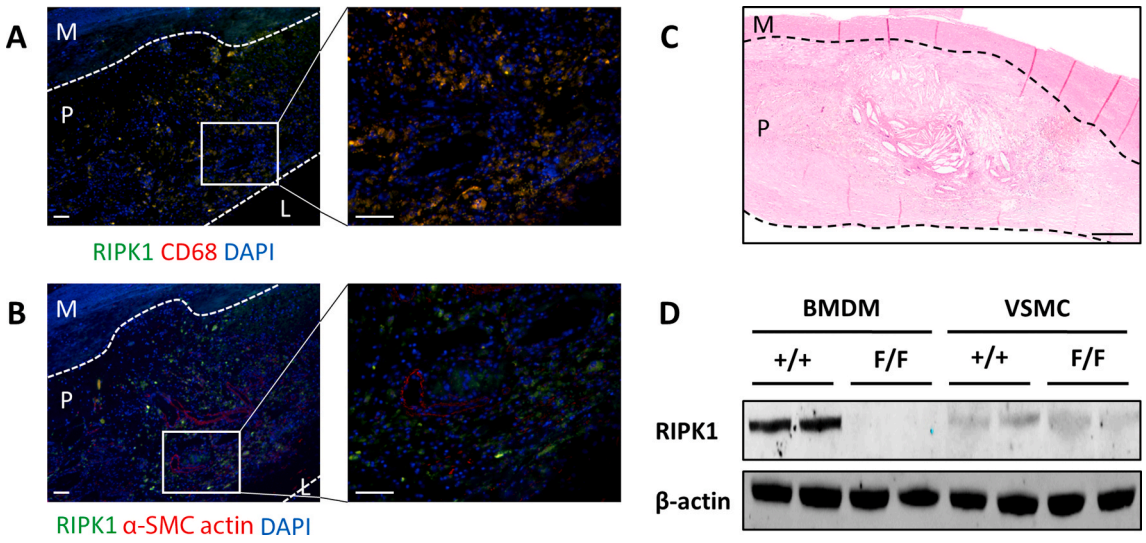

Fig. 1. RIPK1 is highly expressed in macrophages, but not in vascular smooth muscle cells (VSMCs).
(A and B) Double immunofluorescence staining of a human carotid artery lesion showing RIPK1 (green) and CD68 (red) (A), or RIPK1 (green) and α-SMC actin (red) (B). Nuclei were stained with DAPI. L = lumen, M = media, P = plaque. Scale bar = 100 μm. (C) H&E staining of the same human carotid plaque as shown in panels A and B at low magnification. Scale bar = 500 μm. (D) Bone marrow-derived macrophages (BMDM) and vascular smooth muscle cells (VSMC) were isolated from *RIPK1*$^{+/+}$*LysM-Cre*$^{+}$ *ApoE*$^{-/-}$ (+/+) and *RIPK1*$^{F/F}$*LysM-Cre*$^{+}$ *ApoE*$^{-/-}$ (F/F) mice, followed by Western blot analyses of RIPK1 in isolated cells. β-actin was used as loading control.

compared to the ratio at 16 weeks WD, albeit this change did not occur in *RIPK1*$^{F/F}$*LysM-Cre*$^{+}$ *ApoE*$^{-/-}$ mice (Supplementary Fig. 2D). Similar to plaques of *RIPK1*$^{F/F}$*LysM-Cre*$^{+}$ *ApoE*$^{-/-}$ mice after 16 weeks WD, increased TUNEL positivity was associated with a decreased macrophage content (Fig. 3D). Immunoreactivity for cleaved caspase-3 in plaques of *RIPK1*$^{+/+}$*LysM-Cre*$^{+}$ *ApoE*$^{-/-}$ mice (0.38 ± 0.14%) *versus* *RIPK1*$^{F/F}$*LysM-Cre*$^{+}$ *ApoE*$^{-/-}$ mice (0.81 ± 0.26%) was not significantly different (independent samples *t*-test, $p = 0.213$). Moreover, total collagen levels and number of VSMCs did not change between the two groups (Supplementary Fig. 2C and D) and most plaques were negative for neutrophil myeloperoxidase (data not shown).

Because TUNEL staining was elevated in plaques of *RIPK1*$^{F/F}$*LysMCre*$^{+}$ ApoE$^{-/-}$ mice, we investigated the phagocytic clearance of AC, also known as efferocytosis, using double staining for TUNEL and macrophages. The efficiency of efferocytosis was determined by counting the number of free and macrophage-associated AC. After 16 weeks WD, the ratio of free AC/total AC did not differ between atherosclerotic plaques of *RIPK1*$^{F/F}$*LysMCre*$^{+}$ *ApoE*$^{-/-}$ and *RIPK1*$^{+/+}$*LysMCre*$^{+}$ *ApoE*$^{-/-}$ mice (Fig. 4A). However, after 24 weeks WD, the ratio of free AC/total AC significantly increased in atherosclerotic plaques of *RIPK1*$^{F/F}$*LysMCre*$^{+}$ *ApoE*$^{-/-}$ mice as compared to the control mice (Fig. 4A). Moreover, after 24 weeks WD, the ratio of free AC/total AC was significantly increased in atherosclerotic plaques of *RIPK1*$^{F/F}$*LysMCre*$^{+}$ *ApoE*$^{-/-}$ mice as compared to plaques of 16 weeks WD-fed *RIPK1*$^{F/F}$*LysMCre*$^{+}$ *ApoE*$^{-/-}$ mice (Fig. 4A). These data demonstrate that AC in advanced atherosclerotic lesions of *RIPK1*$^{F/F}$*LysMCre*$^{+}$ *ApoE*$^{-/-}$ mice are less efficiently cleared, which eventually may lead to secondary necrosis and plaque progression. To investigate whether *RIPK1* deletion decreases the efferocytosis capacity of BMDM, an *in vitro* efferocytosis assay was performed. Interestingly, RIPK1-deficient BMDM ingested AC as efficiently as control BMDM (Fig. 4B). These finding suggests that the accumulation of AC in plaques of *RIPK1*$^{F/F}$*LysMCre*$^{+}$ *ApoE*$^{-/-}$ mice most likely results from an excessive generation of AC that could not be cleared rather than an inefficient uptake of AC.

3.3. RIPK1 deficiency sensitizes BMDM to undergo apoptosis in vitro

As RIPK1 plays an important role in cell survival via NF-κB-mediated gene induction [16], we treated *RIPK1*$^{+/+}$*LysM-Cre*$^{+}$ *ApoE*$^{-/-}$ and *RIPK1*$^{F/F}$*LysM-Cre*$^{+}$ *ApoE*$^{-/-}$ BMDM with mTNF-α. As shown by Western blotting, phosphorylation (and thus subsequent degradation) of the NF-κB inhibitor IκBα was impaired in mTNF-α-treated *RIPK1*$^{F/F}$*LysM-Cre*$^{+}$ *ApoE*$^{-/-}$ BMDM (Fig. 5A). Similar to cultured BMDM, phosphorylation of NF-κB was significantly inhibited in atherosclerotic tissues of *RIPK1*$^{F/F}$*LysM-Cre*$^{+}$ *ApoE*$^{-/-}$ mice (Fig. 5B), indicating that RIPK1 is essential for NF-κB activation, at least in macrophages. To confirm impaired NF-κB signaling in *RIPK1*$^{+/+}$*LysM-Cre*$^{+}$ *ApoE*$^{-/-}$ *versus* *RIPK1*$^{F/F}$*LysM-Cre*$^{+}$ *ApoE*$^{-/-}$ BMDM, we compared the transcription levels of downstream *NF-κB* gene targets after mTNF-α treatment. Real-time qPCR analysis revealed an increase of both *TNF-α* and *IL-1β* mRNA levels in *RIPK1*$^{+/+}$*LysM-Cre*$^{+}$ *ApoE*$^{-/-}$ BMDM after mTNF-α treatment, which was significantly reduced in mTNF-α-treated *RIPK1*$^{F/F}$*LysM-Cre*$^{+}$ *ApoE*$^{-/-}$ BMDM (Fig. 5C). Interestingly, impaired NF-κB signaling in *RIPK1*$^{F/F}$*LysM-Cre*$^{+}$ *ApoE*$^{-/-}$ BMDM was associated with cleavage of caspase 3 as early as 2 h after mTNF-α treatment followed by cell death induction as shown by increased PI positivity (Fig. 5A and D). Overall, these data demonstrate that RIPK1 deficiency sensitizes BMDM to apoptosis by inhibiting NF-κB activation.

3.4. RIPK1 deficiency does not protect BMDM against necroptosis

RIPK1$^{+/+}$*LysM-Cre*$^{+}$ *ApoE*$^{-/-}$ and *RIPK1*$^{F/F}$*LysM-Cre*$^{+}$ *ApoE*$^{-/-}$ BMDM were treated with LPS and pan-caspase inhibitor zVAD-fmk to induce necroptosis. Both RIPK3 and MLKL were phosphorylated in *RIPK1*$^{+/+}$*LysM-Cre*$^{+}$ *ApoE*$^{-/-}$ BMDM after treatment with LPS/zVAD-fmk, confirming induction of necroptosis. Interestingly, phosphorylation of RIPK3 and MLKL was also observed in LPS/zVAD-fmk-treated *RIPK1*$^{F/F}$*LysM-Cre*$^{+}$ *ApoE*$^{-/-}$ BMDM (Supplementary Fig. 3A). Moreover, both *RIPK1*$^{+/+}$*LysM-Cre*$^{+}$ *ApoE*$^{-/-}$ and *RIPK1*$^{F/F}$*LysM-Cre*$^{+}$ *ApoE*$^{-/-}$ BMDM were characterized by a loss of membrane integrity after LPS/zVAD-fmk treatment as shown by increased PI labeling (Supplementary Fig. 3B). These findings indicate that *RIPK1* deletion is not sufficient to inhibit necroptosis induction by LPS/zVAD-fmk in BMDM. Similar to cultured macrophages, phosphorylation of MLKL was not inhibited in atherosclerotic tissues of *RIPK1*$^{F/F}$*LysM-Cre*$^{+}$ *ApoE*$^{-/-}$ mice. On the contrary, phosphorylation of MLKL was significantly increased in aortic arches of *RIPK1*$^{F/F}$*LysM-Cre*$^{+}$ *ApoE*$^{-/-}$ mice as compared to *RIPK1*$^{+/+}$*LysM-Cre*$^{+}$ *ApoE*$^{-/-}$ mice (Supplementary Fig. 3C). Our data show that

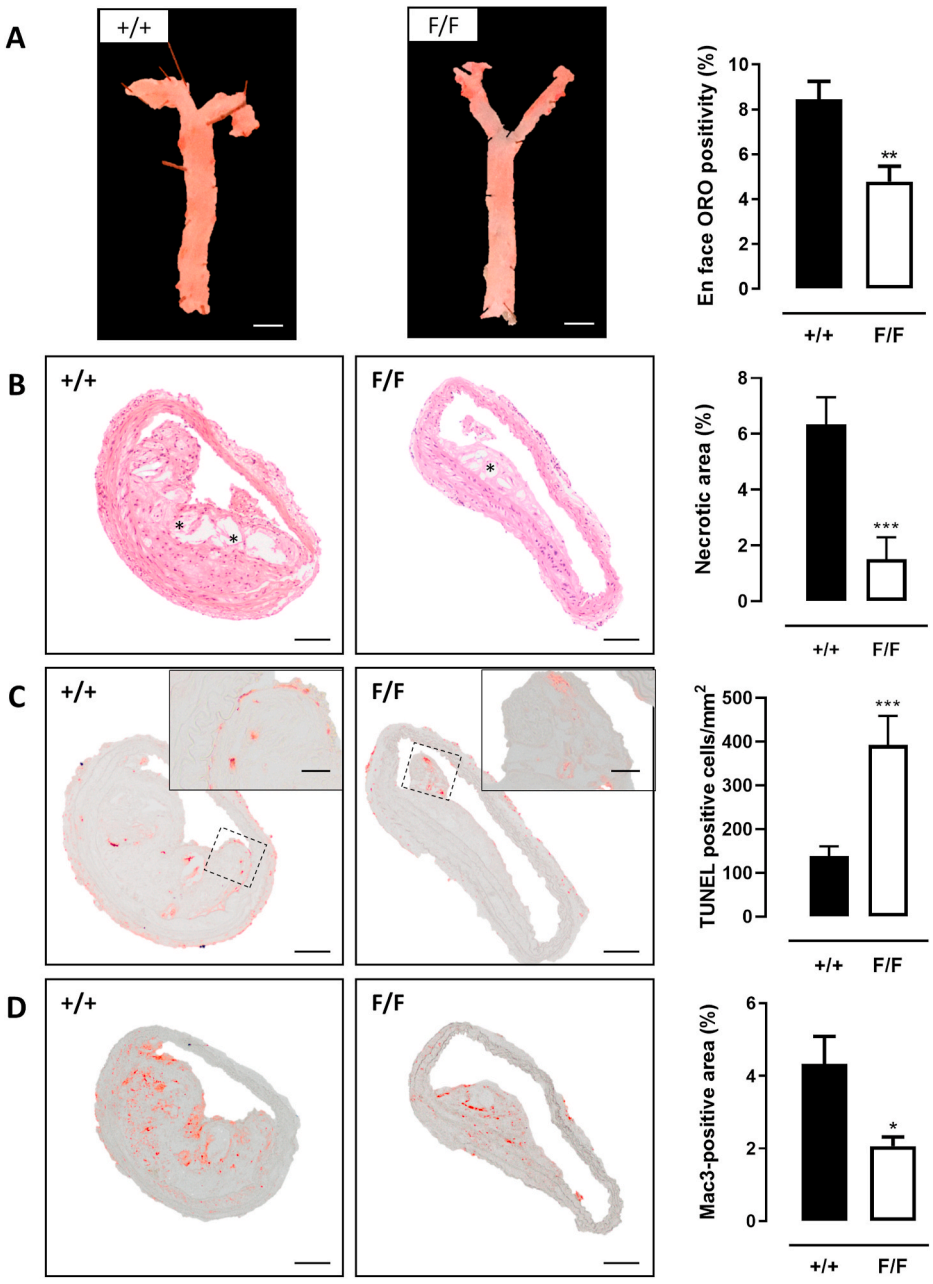

Fig. 2. Myeloid RIPK1 deficiency decreases necrotic core formation and promotes apoptosis in *ApoE*$^{-/-}$ mice after 16 weeks western-type diet. (A) The thoracic aorta and aortic arch of *RIPK1*$^{+/+}$*LysM-Cre*$^{+}$ *ApoE*$^{-/-}$ (+/+) and *RIPK1*$^{F/F}$*LysM-Cre*$^{+}$ *ApoE*$^{-/-}$ (F/F) mice were stained *en face* with Oil Red O to evaluate total plaque burden. $^{**}p < 0.01$ *vs* +/+ (independent samples *t*-test, n = 6 for both groups). Scale bar = 5 mm. (B–D) Sections of the brachiocephalic artery of *RIPK1*$^{+/+}$*LysMCre*$^{+}$ *ApoE*$^{-/-}$ (+/+) and *RIPK1*$^{F/F}$*LysMCre*$^{+}$ *ApoE*$^{-/-}$ (F/F) mice were stained with (B) H&E to quantify plaque necrosis (the necrotic core is indicated by asterisks), (C) TUNEL to detect apoptotic cells and (D) anti-Mac-3 to determine macrophage content. Inserts in panel C represent magnifications of the boxed areas (scale bar = 25 μm). $^{*}p < 0.05$, $^{***}p < 0.001$ *vs* +/+ (Mann-Whitney *U* test, n = 17–20 for both groups). Scale bar = 100 μm. Representative images are shown.

loss of RIPK1 does not protect but potentiates RIPK3-MLKL-dependent necroptosis in macrophages *in vitro* and *in vivo*.

4. Discussion

The role of RIPK1 has been studied in different inflammatory diseases including colitis [28], skin inflammation [29], myocardial infarction [30], hepatitis [31] and ischemic organ injury [32] but its role in atherosclerosis is still unknown. We show that RIPK1 is highly expressed in macrophages of human carotid plaques and elucidate the complex role of myeloid RIPK1 in atherosclerotic plaque development. Our data demonstrate that deletion of *RIPK1* in myeloid cells using *RIPK1*$^{F/F}$*LysM-Cre*$^{+}$ *ApoE*$^{-/-}$ mice results in reduced plaque formation in the descending aorta and brachiocephalic artery after 16 weeks western-type diet (WD). Myeloid *RIPK1* deletion reduced plaque area and necrotic core without affecting total collagen level and the amount of VSMCs. Moreover, the reduction in plaque size and necrotic core in plaques of *RIPK1*$^{F/F}$*LysM-Cre*$^{+}$ *ApoE*$^{-/-}$ mice was associated with a significant decrease in macrophage content while TUNEL staining increased. Indeed, *in vitro* experiments demonstrated that NF-κB-mediated cell survival is impaired in *RIPK1*$^{F/F}$*LysM-Cre*$^{+}$*ApoE*$^{-/-}$ macrophages when exposed to TNF-α, and rapidly triggers *RIPK1*$^{F/F}$*LysM-Cre*$^{+}$*ApoE*$^{-/-}$ macrophage death via caspase 3-dependent apoptosis. Our results confirm previous findings that knocking out RIPK1 in macrophages leads to TNF-α-dependent apoptotic death [33]. The observed switch between cell survival and death in the absence of RIPK1 is most likely induced by the reduced NF-κB-mediated transcription of a number of pro-survival genes, most important among these being FLICE-like inhibitory protein (cFLIP), cIAP1/2 and A20 [15, 34–36]. Importantly, the enhanced TUNEL staining in plaques of *RIPK1*$^{F/F}$*LysM-Cre*$^{+}$ *ApoE*$^{-/-}$ mice did not correlate with more abundant cleaved capase-3 positive cells. TUNEL is a widely used marker of apoptotic cell death, but may in some cases reflect necrotic cell death rather than apoptosis. Given that the size of necrotic cores is reduced in

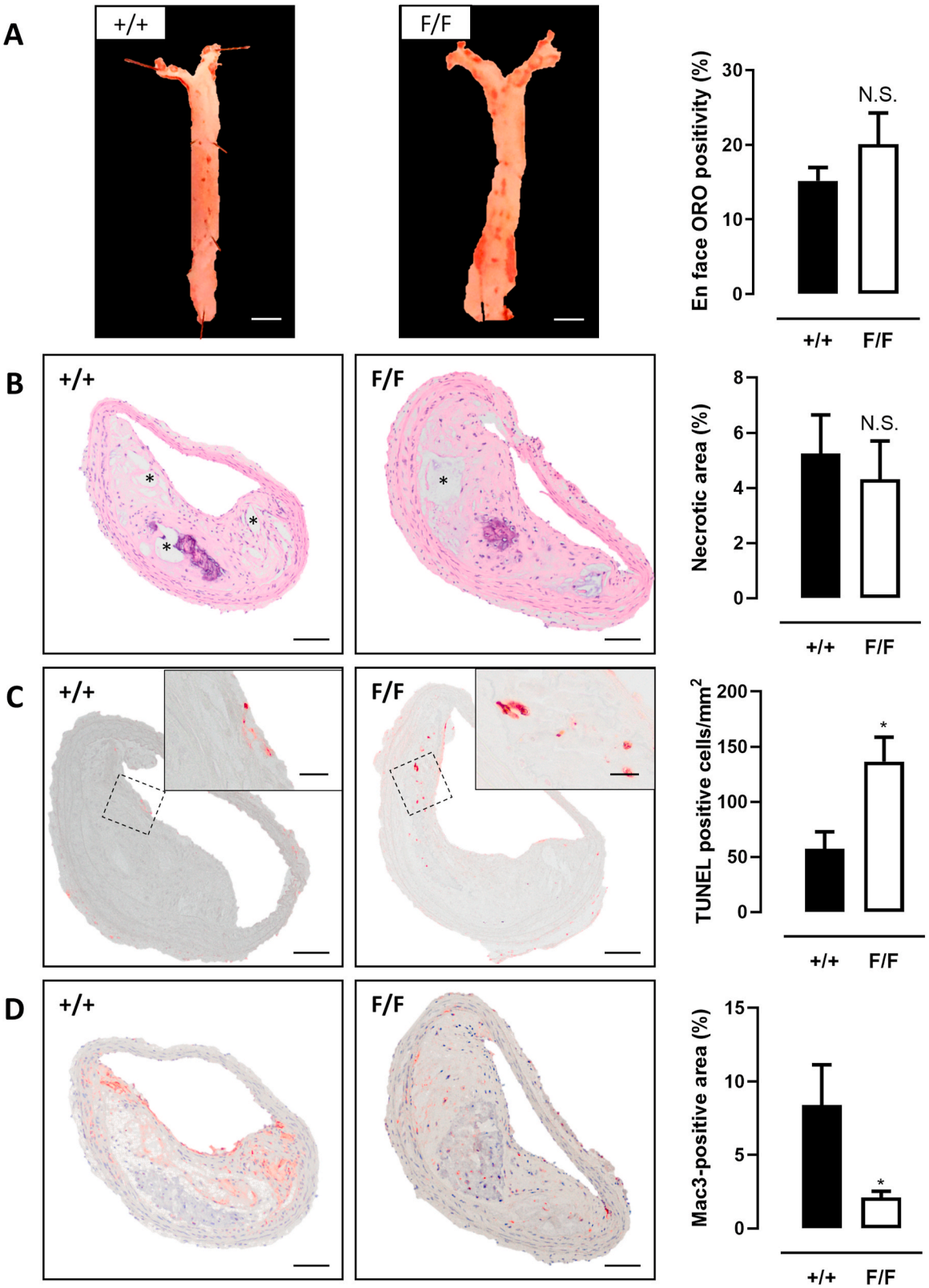

Fig. 3. Myeloid RIPK1 deficiency induces apoptosis and decreases macrophage content in *ApoE*$^{-/-}$ mice after 24 weeks western-type diet.
(A) The thoracic aorta and aortic arch of *RIPK1*$^{+/+}$*LysM-Cre*$^{+}$ *ApoE*$^{-/-}$ (+/+) and *RIPK1*$^{F/F}$*LysM-Cre*$^{+}$ *ApoE*$^{-/-}$ (F/F) mice were stained *en face* with Oil Red O to evaluate total plaque burden. N.S., not significant (independent samples *t*-test, n = 6 for both groups). Scale bar = 5 mm. (B–D) Sections of the brachiocephalic artery of *RIPK1*$^{+/+}$*LysMCre*$^{+}$ *ApoE*$^{-/-}$ (+/+) and *RIPK1*$^{F/F}$*LysMCre*$^{+}$ *ApoE*$^{-/-}$ (F/F) mice were stained with (B) H&E to quantify plaque necrosis (the necrotic core is indicated by an asterisk), (C) TUNEL to detect apoptotic cells and (D) anti-Mac-3 to determine macrophage content. Inserts in panel C represent magnifications of the boxed areas (scale bar = 25 μm). *$p < 0.05$ vs +/+ (Mann-Whitney *U* test, n = 8–10 for both groups). N.S., not significant. Scale bar = 100 μm. Representative images are shown.

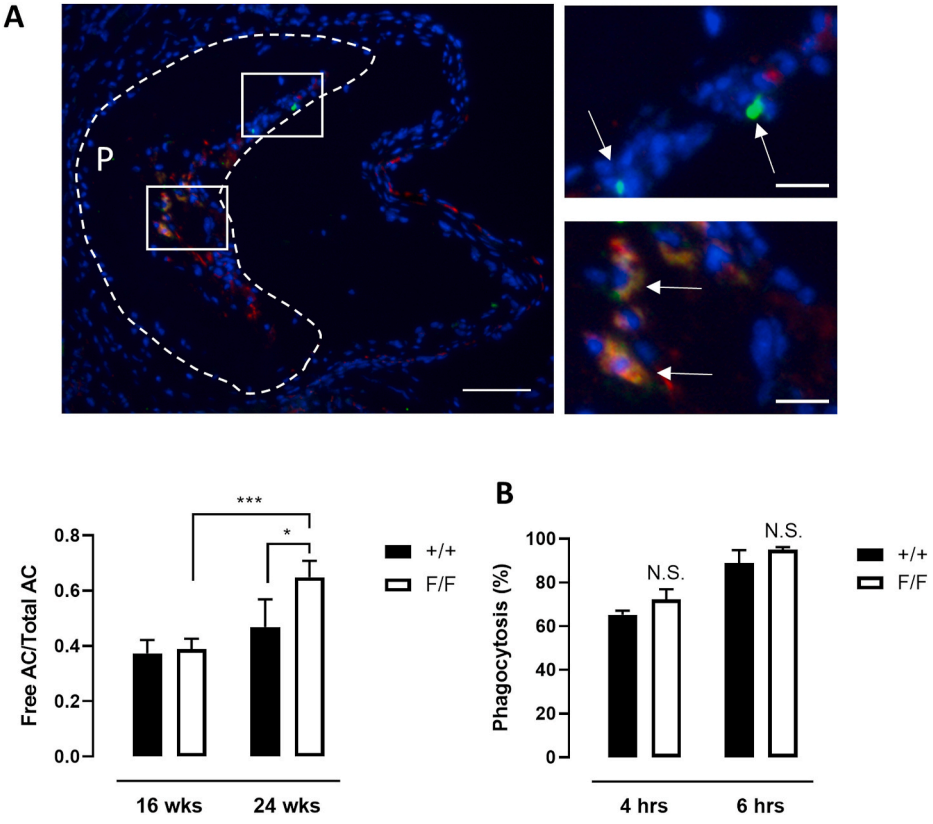

Fig. 4. Efferocytosis is impaired in advanced atherosclerotic plaques of *RIPK1*$^{F/F}$*LysM-Cre*$^{+}$ *ApoE*$^{-/-}$ after 24 weeks western-type diet.
(A) *RIPK1*$^{+/+}$*LysM-Cre*$^{+}$ *ApoE*$^{-/-}$ (+/+) and *RIPK1*$^{F/F}$*LysM-Cre*$^{+}$ *ApoE*$^{-/-}$ (F/F) mice were fed a western-type diet for 16 weeks or 24 weeks. A representative image of an aortic root of a *RIPK1*$^{F/F}$*LysM-Cre*$^{+}$ *ApoE*$^{-/-}$ mouse after 24 weeks western-type diet is shown, in which apoptotic cells (AC) were labeled by TUNEL (green), macrophages by anti-CD68 (red) and nuclei by DAPI (blue). P = plaque. High power magnifications of the boxed areas are also displayed. Examples of free AC (top magnification) and phagocytized AC (bottom magnification) are indicated by white arrows. The graph shows quantification of the ratio of free to total AC. *$p < 0.05$, ***$p < 0.001$ (three-way ANOVA followed by Bonferroni's *post hoc* test, 16 weeks n = 17–20, 24 weeks n = 8–10). Scale bar = 100 μm (low power micrograph) or 20 μm (high power micrographs). (B) Bone-marrow-derived macrophages were isolated from *RIPK1*$^{+/+}$*LysM-Cre*$^{+}$ *ApoE*$^{-/-}$ (+/+) and *RIPK1*$^{F/F}$*LysM-Cre*$^{+}$ *ApoE*$^{-/-}$ (F/F) mice. AC were generated by treating U937 cells with 50 μM etoposide for 4 or 6 h. Phagocytosis of AC was measured via flow cytometry after pre-incubation of macrophages for 1 h with apoptotic U937 cells. N.S., not significant *vs* +/+ (independent samples *t*-test, n = 4).

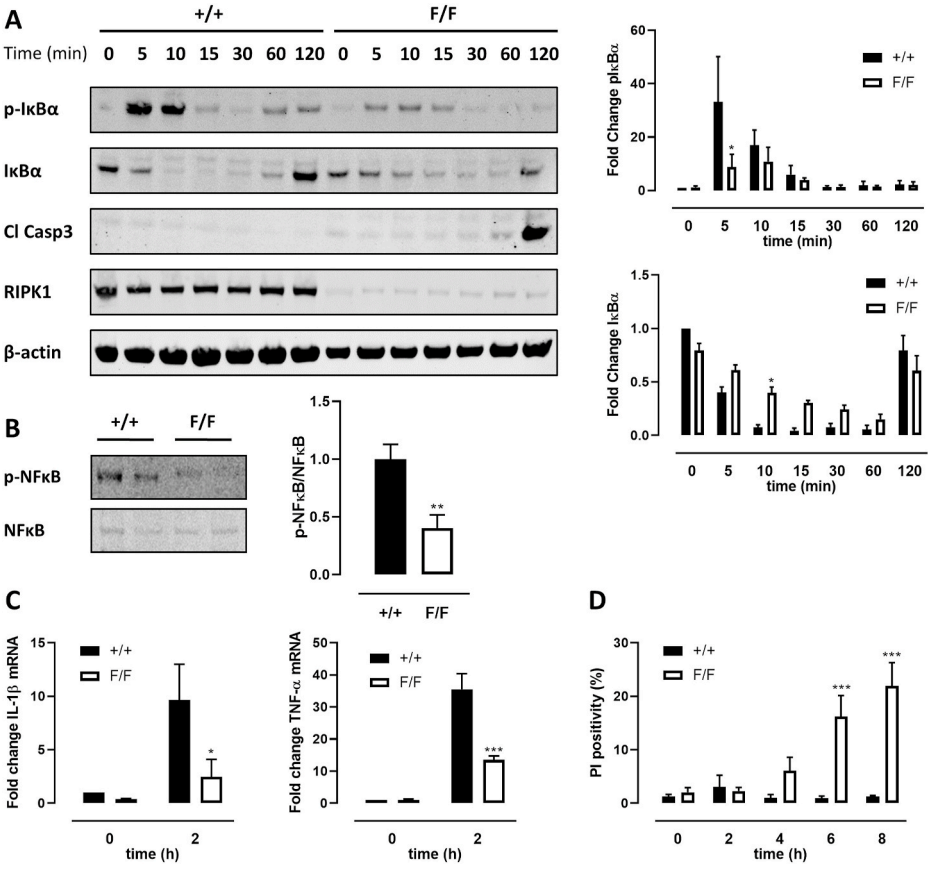

Fig. 5. RIPK1 deficiency sensitizes macrophages to undergo apoptosis.
(A) Bone marrow-derived macrophages (BMDM) were isolated from *RIPK1*$^{+/+}$*LysM-Cre*$^{+}$ *ApoE*$^{-/-}$ (+/+) and *RIPK1*$^{F/F}$*LysM-Cre*$^{+}$ *ApoE*$^{-/-}$ (F/F) mice. BMDM were treated with 50 ng/mL mTNF-α for the indicated timeframe. Western blot analysis for p-IκBα, IκBα, cleaved caspase 3 and RIPK1 (β-actin was used as loading control). *$p < 0.05$ *vs* +/+ (two-way ANOVA followed by Bonferroni's post hoc test, n = 3). (B) Western blot analysis for p–NF–κB and NF-κB in lysates of the aortic arch from *RIPK1*$^{+/+}$*LysM-Cre*$^{+}$ *ApoE*$^{-/-}$ (+/+) and *RIPK1*$^{F/F}$*LysM-Cre*$^{+}$ *ApoE*$^{-/-}$ (F/F) mice fed a western-type diet for 16 weeks. **$p < 0.01$ *vs* +/+ (independent samples *t*-test, n = 7–10 for both groups). (C and D) *RIPK1*$^{+/+}$*LysM-Cre*$^{+}$ *ApoE*$^{-/-}$ (+/+) and *RIPK1*$^{F/F}$*LysM-Cre*$^{+}$ *ApoE*$^{-/-}$ (F/F) BMDM were treated with 50 ng/mL mTNF-α for the indicated timeframe. (C) Real-time RT-PCR analysis of *TNF-α* and *IL-1β* mRNA (β-actin and peptidyl isomerase A were used as housekeeping genes). *$p < 0.05$, ***$p < 0.001$ *vs* +/+ (two-way ANOVA followed by Bonferroni's *post hoc* test, n = 4 independent experiments in triplicate). (D) Monitoring of cell death via PI labelling. ***$p < 0.001$ *vs* +/+ (two-way ANOVA followed by Bonferroni's *post hoc* test, n = 3).

plaques of *RIPK1*$^{F/F}$*LysM-Cre*$^{+}$ *ApoE*$^{-/-}$ mice (after 16 weeks WD) while TUNEL is strongly increased, this seems highly unlikely. Previous reports indicate that staining for cleaved caspase-3 may give an underestimation of the actual apoptosis frequency because cleaved caspase-3 is rapidly degraded and thus difficult to detect [37]. Overall, our results show that myeloid RIPK1 controls a fine balance between NF-κB-dependent survival and cell death, while loss of RIPK1 triggers TNFα-induced macrophage apoptosis.

The abovementioned findings are in line with previous observations in mice lacking cell survival proteins. For example, deletion of apoptosis inhibitor of macrophage (AIM) suppresses atherosclerotic plaque development by increasing macrophage apoptosis in *Ldlr*$^{-/-}$ mice [38]. Knocking out cellular inhibitor of apoptosis 2 (cIAP2) increases macrophage apoptosis and reduces atherosclerosis burden in *ApoE*$^{-/-}$ mice [39]. IKKα deficiency in mouse macrophages compromises cell resistance to pro-apoptotic stimuli and reduces early atherosclerosis in *Ldlr*$^{-/-}$ mice [40]. Overall, these studies indicate that macrophage apoptosis decreases lesion cellularity and attenuates plaque progression in early stages of atherosclerosis. These studies also imply that phagocytic clearance of AC, better known as efferocytosis, is efficient in early lesions.

To further examine the consequences of myeloid RIPK1 deficiency in atherosclerotic lesions after prolonged WD feeding, *RIPK1*$^{F/F}$*LysM-Cre*$^{+}$ *ApoE*$^{-/-}$ and *RIPK1*$^{+/+}$*LysM-Cre*$^{+}$ *ApoE*$^{-/-}$ mice were fed a WD for 24 weeks. Interestingly, after 24 weeks WD, plaque size and necrosis were no longer different between both groups. While the large plaques of *RIPK1*$^{+/+}$*LysM-Cre*$^{+}$ *ApoE*$^{-/-}$ mice did not further increase in size, *RIPK1*$^{F/F}$*LysM-Cre*$^{+}$ *ApoE*$^{-/-}$ mice showed accelerated plaque formation between 16 and 24 weeks WD. The ratio maximum fibrous cap thickness/maximum plaque thickness significantly decreased in *RIPK1*$^{+/+}$*LysM-Cre*$^{+}$ *ApoE*$^{-/-}$ mice, but not in *RIPK1*$^{F/F}$*LysM-Cre*$^{+}$ *ApoE*$^{-/-}$ mice. This finding together with the smaller plaques of *RIPK1*$^{F/F}$*LysM-Cre*$^{+}$ *ApoE*$^{-/-}$ mice at 16 weeks WD suggest that formation and destabilization of plaques occur faster in *RIPK1*$^{+/+}$*LysM-Cre*$^{+}$ *ApoE*$^{-/-}$ mice. Interestingly, free AC accumulated in plaques of *RIPK1*$^{F/F}$*LysM-Cre*$^{+}$ *ApoE*$^{-/-}$ mice after 24 weeks WD, suggestive of defective AC clearance. Indeed, numerous studies have shown that efferocytosis is impaired in advanced atherosclerotic plaques [4,41]. Most likely, free AC in plaques of *RIPK1*$^{F/F}$*LysM-Cre*$^{+}$ *ApoE*$^{-/-}$ mice underwent secondary necrosis as a result of impaired clearance, thereby contributing to plaque progression and the formation and enlargement of the necrotic core [2]. Even though the incidence of apoptosis in plaques of *RIPK1*$^{F/F}$*LysM-Cre*$^{+}$ *ApoE*$^{-/-}$ mice decreased between 16 and 24 weeks WD, the necrotic core area concomitantly increased two-fold. These data strongly imply that accumulation of free AC in plaques of *RIPK1*$^{F/F}$*LysM-Cre*$^{+}$ *ApoE*$^{-/-}$ mice promotes necrotic core formation, illustrating the dynamics of RIPK1-mediated macrophage cell death in plaque progression.

Next to secondary necrosis, myeloid *RIPK1* deletion did not protect macrophages against necroptosis, indicating that RIPK1, unlike RIPK3 [12,42], is dispensable for necroptosis. In fact, myeloid RIPK1 deficiency in *ApoE*$^{-/-}$ mice upregulate necroptosis in atherosclerotic plaques as demonstrated by elevated levels of phosphorylated MLKL. An upregulation of necroptosis has been previously reported in mice lacking RIPK1 in the epidermis. Keratinocytes of these mice showed increased necroptosis mediated by the engagement of RIPK3 with Z-DNA binding protein 1 (ZBP1), and to a lesser extent with TIR domain containing adaptor inducing IFN-β (TRIF) through common RIP homotypic interaction motifs (RHIM) [29,43,44]. Furthermore, accelerated necroptosis regulated by the TRADD-RIPK3-MLKL pathway has been reported in TNF-α-treated L929 and HT-22 cells lacking RIPK1 [45,46]. The molecular mechanisms underlying necroptosis induction in advanced atherosclerotic plaques are unclear. Necroptosis can be induced by different ligands such as TNF, TRAIL, TWEAK and CD95L that bind to their respective death receptors. It has been suggested that the underlying mechanism of necroptosis in the plaque involves oxLDL [11]. However, only when caspase-8 is absent or inactive, necroptosis is initiated [47]. Caspases can be inactivated in plaques by oxidation or S-nitrosylation of a critical thiol residue in the active site [48,49]. We hypothesize that inducible nitric oxide synthase (iNOS)-driven S-nitrosylation (i.e. inactivation) of caspase-8 (a key factor in the necroptosis pathway), in combination with pro-apoptotic signaling, may trigger necroptosis and necrotic core formation. Previous studies revealed that macrophages overexpressing iNOS frequently surround the necrotic core of human plaques [50], which favors this hypothesis.

Based on the abovementioned findings, both the upregulation of necroptosis, as well as the secondary necrosis of free AC, is likely responsible for the enlargement of the necrotic core in *RIPK1*$^{F/F}$*LysM-Cre*$^{+}$ *ApoE*$^{-/-}$ mice. However, it was previously reported that the RIPK1 inhibitor Nec-1s reduces lesion progression and plaque vulnerability by necroptosis inhibition [11]. The differences between the studies can be explained by a number of reasons. Firstly, Nec-1s inhibits the kinase function of RIPK1, but does not interfere with its scaffold function [51], while genetic disruption of RIPK1 affects both its kinase activity and scaffold function. Indeed, pharmacological inhibition of RIPK1 by Nec-1 has been shown to inhibit TNF-α-induced necroptosis, while knockdown of RIPK1 can potentiate this process [46]. Secondly, the effect of Nec-1s was only studied after 10 weeks of diet and so its effect on more advanced (24 weeks WD) plaques is not known. Thirdly, the authors did not report a reduction in macrophage content, nor was plaque apoptosis examined [11]. Instead, the authors observed an increase in VSMC content, suggesting that the mechanism by which Nec-1s impacts atherosclerosis, including various plaque cell types, differs from *RIPK1* gene deletion. Finally, the difference in plaque composition could be due to the study of different vascular beds (aortic root *vs.* brachiocephalic artery plaques).

Another factor that may significantly contribute to plaque progression in *RIPK1*$^{F/F}$*LysM-Cre*$^{+}$*ApoE*$^{-/-}$ mice at later time points (24 weeks WD) is the relatively high level of plasma cholesterol *versus* *RIPK1*$^{+/+}$*LysM-Cre*$^{+}$*ApoE*$^{-/-}$ mice. According to recent evidence, inhibition of RIPK1 suppresses the expression of a set of genes including *Ch25h* that encodes cholesterol 25-hydroxylase [52]. Because Ch25h enzyme downregulates cholesterol synthesis, Ch25h inhibition by *RIPK1* deletion elevates plasma cholesterol levels. In addition, knocking down RIPK1 in macrophages increases the expression of ATP-binding cassette transporter ABCA1 [53], also known as the cholesterol efflux regulatory protein (CERP), suggesting that this condition promotes reverse cholesterol transport, increased levels of plasma cholesterol and plaque progression.

Very recently, Karunakaran et al. [54] reported that *RIPK1* silencing in *ApoE*$^{-/-}$ mice using weekly injections of antisense oligonucleotides inhibits plaque formation. In contrast to cell-specific *RIPK1* gene deletion, knocking down RIPK1 via antisense oligonucleotides promotes neither spontaneous cell death nor changes in plasma cholesterol, but abrogates excessive NF-κB activation (without completely inactivating it).The authors claim that plaque progression is dramatically reduced by directly inhibiting NF-κB inflammatory signaling and the secretion of proinflammatory cytokines including IL-1α and IL-1β [54], which is obviously an attractive approach to dampen atherosclerotic vascular disease.

In conclusion, myeloid RIPK1 has divergent effects on atherosclerosis depending on the lesion stage. Myeloid *RIPK1* gene deletion limits plaque progression after 16 weeks WD through induction of apoptosis but promotes accumulation of free AC, secondary necrosis and necroptosis after 24 weeks WD.

Financial support

This work was supported by the Fund for Scientific Research (FWO)-Flanders (EOS 30826052). Isabelle Coornaert and Pauline Puylaert are fellows of the FWO-Flanders. Research in the Vandenabeele group is supported by EOS MODEL-IDI (30826052), FWO research grants (G.0E04.16N, G.0C76.18N, G.0B71.18N, G.0B96.20N), Methusalem

(BOF16/MET_V/007), the Belgian Foundation against Cancer (FAF-F/2016/865), the Cancer Research Institute Ghent (CRIG), the Ghent Gut Inflammation Group (GGIG) and VIB (Vlaams Instituut voor Biotechnologie).

CRediT author statement

Isabelle Coornaert: investigation, formal analysis, writing – original draft, visualization; **Pauline Puylaert:** investigation, formal analysis, visualization; **Giullia Marcasolli:** investigation; **Mandy O.J. Grootaert:** methodology, writing – review & editing; **Peter Vandenabeele:** conceptualization, resources, writing – review and editing, funding acquisition; **Guido R.Y. De Meyer:** conceptualization, formal analysis, writing – original draft, writing – review & editing, supervision, funding acquisition; **Wim Martinet:** conceptualization, writing – original draft, writing – review & editing, supervision, funding aquisition.

Declaration of competing interest

The authors declare that they have no known competing financial interests or personal relationships that could have appeared to influence the work reported in this paper.

Acknowledgements

The authors are grateful to Dr. Bronwen Martin for critical reading of the manuscript. The authors thank Dr Bart Peeters, Rita Van den Bossche, Mandy Vermont, Hermine Fret and Anne-Elise Van Hoydonck for excellent technical support.

Appendix A. Supplementary data

Supplementary data to this article can be found online at https://doi.org/10.1016/j.atherosclerosis.2021.02.021.

References

[1] A.J. Lusis, Atherosclerosis, Nature 407 (6801) (2000) 233–241.
[2] W. Martinet, D. Schrijvers, G.R.Y. De Meyer, Necrotic cell death in atherosclerosis, Basic Res. Cardiol. 106 (5) (2011) 749–760.
[3] W. Martinet, I. Coornaert, P. Puylaert, G.R.Y. De Meyer, Macrophage death as a pharmacological target in atherosclerosis, Front. Pharmacol. 10 (2019), 306-306.
[4] D.M. Schrijvers, G.R.Y. De Meyer, M.M. Kockx, A.G. Herman, et al., Phagocytosis of apoptotic cells by macrophages is impaired in atherosclerosis, Arterioscler. Thromb. Vasc. Biol. 25 (6) (2005) 1256–1261.
[5] N. Kalinina, A. Agrotis, Y. Antropova, G. DiVitto, et al., Increased expression of the DNA-binding cytokine HMGB1 in human atherosclerotic lesions: role of activated macrophages and cytokines, Arterioscler. Thromb. Vasc. Biol. 24 (12) (2004) 2320–2325.
[6] B. Lundberg, Chemical composition and physical state of lipid deposits in atherosclerosis, Atherosclerosis 56 (1) (1985) 93–110.
[7] Y. Cho, S. Challa, D. Moquin, R. Genga, et al., Phosphorylation-driven assembly of the RIP1-RIP3 complex regulates programmed necrosis and virus-induced inflammation, Cell 137 (6) (2009) 1112–1123.
[8] Y. Dondelinger, W. Declercq, S. Montessuit, R. Roelandt, et al., MLKL compromises plasma membrane integrity by binding to phosphatidylinositol phosphates, Cell Rep. 7 (4) (2014) 971–981.
[9] H. Wang, L. Sun, L. Su, J. Rizo, et al., Mixed lineage kinase domain-like protein MLKL causes necrotic membrane disruption upon phosphorylation by RIP3, Mol. Cell. 54 (1) (2014) 133–146.
[10] F. Tian, J. Yao, M. Yan, X. Sun, et al., 5-Aminolevulinic acid-mediated sonodynamic therapy inhibits RIPK1/RIPK3-dependent necroptosis in THP-1-derived foam cells, Sci. Rep. 6 (2016) 21992.
[11] D. Karunakaran, M. Geoffrion, L. Wei, W. Gan, et al., Targeting macrophage necroptosis for therapeutic and diagnostic interventions in atherosclerosis, Science Advances 2 (7) (2016), e1600224.
[12] J. Lin, H. Li, M. Yang, J. Ren, et al., A role of RIP3-mediated macrophage necrosis in atherosclerosis development, Cell Rep. 3 (1) (2013) 200–210.
[13] Rasheed A, Robichaud S, Nguyen M-A, Geoffrion M, et al. Loss of MLKL (mixed lineage kinase-like domain protein) decreases necrotic core but increases macrophage lipid accumulation in atherosclerosis. Arterioscler. Thromb. Vasc. Biol.. 0(0): p. ATVBAHA.119.313640.
[14] M.A. Kelliher, S. Grimm, Y. Ishida, F. Kuo, et al., The death domain kinase RIP mediates the TNF-induced NF-kappaB signal, Immunity 8 (3) (1998) 297–303.
[15] L. Wang, F. Du, X. Wang, TNF-alpha induces two distinct caspase-8 activation pathways, Cell 133 (4) (2008) 693–703.
[16] W. Declercq, T. Vanden Berghe, P. Vandenabeele, RIP kinases at the crossroads of cell death and survival, Cell 138 (2) (2009) 229–232.
[17] L. Mifflin, D. Ofengeim, J. Yuan, Receptor-interacting protein kinase 1 (RIPK1) as a therapeutic target, Nat. Rev. Drug Discov. 19 (8) (2020) 553–571.
[18] Y. Dondelinger, T. Delanghe, D. Priem, M.A. Wynosky-Dolfi, et al., Serine 25 phosphorylation inhibits RIPK1 kinase-dependent cell death in models of infection and inflammation, Nat. Commun. 10 (1) (2019) 1729.
[19] Y. Dondelinger, M. Darding, M.J. Bertrand, H. Walczak, Poly-ubiquitination in TNFR1-mediated necroptosis, Cell. Mol. Life Sci. 73 (11–12) (2016) 2165–2176.
[20] M.J. Bertrand, S. Milutinovic, K.M. Dickson, W.C. Ho, et al., cIAP1 and cIAP2 facilitate cancer cell survival by functioning as E3 ligases that promote RIP1 ubiquitination, Mol. Cell. 30 (6) (2008) 689–700.
[21] M.A. O'Donnell, D. Legarda-Addison, P. Skountzos, W.C. Yeh, et al., Ubiquitination of RIP1 regulates an NF-kappaB-independent cell-death switch in TNF signaling, Curr. Biol. 17 (5) (2007) 418–424.
[22] T. Delanghe, Y. Dondelinger, M.J.M. Bertrand, RIPK1 kinase-dependent death: a symphony of phosphorylation events, Trends Cell Biol. 30 (3) (2020) 189–200.
[23] N. Takahashi, L. Vereecke, M.J.M. Bertrand, L. Duprez, et al., RIPK1 ensures intestinal homeostasis by protecting the epithelium against apoptosis, Nature 513 (7516) (2014) 95–99.
[24] A. Kurdi, L. Roth, B. Van der Veken, D. Van Dam, et al., Everolimus depletes plaque macrophages, abolishes intraplaque neovascularization and improves survival in mice with advanced atherosclerosis, Vasc. Pharmacol. 113 (2019) 70–76.
[25] G. Owens, A. Loeb, D. Gordon, M. Thompson, Expression of smooth muscle-specific alpha-isoactin in cultured vascular smooth muscle cells: relationship between growth and cytodifferentiation, J. Cell Biol. 102 (2) (1986) 343–352.
[26] A.A. Geisterfer, M.J. Peach, G.K. Owens, Angiotensin II induces hypertrophy, not hyperplasia, of cultured rat aortic smooth muscle cells, Circ. Res. 62 (4) (1988) 749–756.
[27] D.M. Schrijvers, W. Martinet, G.R.Y. De Meyer, L. Andries, et al., Flow cytometric evaluation of a model for phagocytosis of cells undergoing apoptosis, J. Immunol. Methods 287 (1) (2004) 101–108.
[28] H. Lu, H. Li, C. Fan, Q. Qi, et al., RIPK1 inhibitor ameliorates colitis by directly maintaining intestinal barrier homeostasis and regulating following IECs-immuno crosstalk, Biochem. Pharmacol. 172 (2020) 113751.
[29] J. Lin, S. Kumari, C. Kim, T.-M. Van, et al., RIPK1 counteracts ZBP1-mediated necroptosis to inhibit inflammation, Nature 540 (7631) (2016) 124–128.
[30] H. Tan, J. Qi, B.Y. Fan, J. Zhang, et al., MicroRNA-24-3p attenuates myocardial ischemia/reperfusion injury by suppressing RIPK1 expression in mice, Cell. Physiol. Biochem. 51 (1) (2018) 46–62.
[31] A. Filliol, C. Piquet-Pellorce, J. Le Seyec, M. Farooq, et al., RIPK1 protects from TNF-α-mediated liver damage during hepatitis, Cell Death Dis. 7 (11) (2016) e2462-e2462.
[32] H. Zhao, T. Jaffer, S. Eguchi, Z. Wang, et al., Role of necroptosis in the pathogenesis of solid organ injury, Cell Death Dis. 6 (11) (2015) e1975-e1975.
[33] J. Buchrieser, M.J. Oliva-Martin, M.D. Moore, J.C.D. Long, et al., RIPK1 is a critical modulator of both tonic and TLR-responsive inflammatory and cell death pathways in human macrophage differentiation, Cell Death Dis. 9 (10) (2018) 973.
[34] O. Micheau, J. Tschopp, Induction of TNF receptor I-mediated apoptosis via two sequential signaling complexes, Cell 114 (2) (2003) 181–190.
[35] D. Priem, M. Devos, S. Druwé, A. Martens, et al., A20 protects cells from TNF-induced apoptosis through linear ubiquitin-dependent and -independent mechanisms, Cell Death Dis. 10 (10) (2019) 692.
[36] C.Y. Wang, M.W. Mayo, R.G. Korneluk, D.V. Goeddel, et al., NF-kappaB antiapoptosis: induction of TRAF1 and TRAF2 and c-IAP1 and c-IAP2 to suppress caspase-8 activation, Science 281 (5383) (1998) 1680–1683.
[37] P. Tawa, K. Hell, A. Giroux, E. Grimm, et al., Catalytic activity of caspase-3 is required for its degradation: stabilization of the active complex by synthetic inhibitors, Cell Death Differ. 11 (4) (2004) 439–447.
[38] S. Arai, J.M. Shelton, M. Chen, M.N. Bradley, et al., A role for the apoptosis inhibitory factor AIM/Spalpha/Api6 in atherosclerosis development, Cell Metabol. 1 (3) (2005) 201–213.
[39] L. Sleiman, R. Beanlands, M. Hasu, M. Thabet, et al., Loss of cellular inhibitor of apoptosis protein 2 reduces atherosclerosis in atherogenic apoE-/- C57BL/6 mice on high-fat diet, Journal of the American Heart Association 2 (5) (2013) e000259-e000259.
[40] V.R. Babaev, L. Ding, Y. Zhang, J.M. May, et al., Macrophage IKKalpha deficiency suppresses akt phosphorylation, reduces cell survival, and decreases early atherosclerosis, Arterioscler. Thromb. Vasc. Biol. 36 (4) (2016) 598–607.
[41] I. Tabas, Consequences and therapeutic implications of macrophage apoptosis in atherosclerosis: the importance of lesion stage and phagocytic efficiency, Arterioscler. Thromb. Vasc. Biol. 25 (11) (2005) 2255–2264.
[42] L. Meng, W. Jin, X. Wang, RIP3-mediated necrotic cell death accelerates systematic inflammation and mortality, Proc. Natl. Acad. Sci. Unit. States Am. 112 (35) (2015), 11007.
[43] M. Dannappel, K. Vlantis, S. Kumari, A. Polykratis, et al., RIPK1 maintains epithelial homeostasis by inhibiting apoptosis and necroptosis, Nature 513 (7516) (2014) 90–94.
[44] M. Devos, G. Tanghe, B. Gilbert, E. Dierick, et al., Sensing of endogenous nucleic acids by ZBP1 induces keratinocyte necroptosis and skin inflammation, J. Exp. Med. 217 (7) (2020).

[45] L. Wang, X. Chang, J. Feng, J. Yu, et al., TRADD mediates RIPK1-independent necroptosis induced by tumor necrosis factor, Frontiers in cell and developmental biology 7 (2020), 393-393.
[46] C.J. Kearney, S.P. Cullen, D. Clancy, S.J. Martin, RIPK1 can function as an inhibitor rather than an initiator of RIPK3-dependent necroptosis, FEBS J. 281 (21) (2014) 4921–4934.
[47] S. Grootjans, T. Vanden Berghe, P. Vandenabeele, Initiation and execution mechanisms of necroptosis: an overview, Cell Death Differ. 24 (7) (2017) 1184–1195.
[48] V. Borutaite, G.C. Brown, Caspases are reversibly inactivated by hydrogen peroxide, FEBS Lett. 500 (3) (2001) 114–118.
[49] J. Li, T.R. Billiar, R.V. Talanian, Y.M. Kim, Nitric oxide reversibly inhibits seven members of the caspase family via S-nitrosylation, Biochem. Biophys. Res. Commun. 240 (2) (1997) 419–424.
[50] K.M. Cromheeke, M.M. Kockx, G.R.Y. De Meyer, J.M. Bosmans, et al., Inducible nitric oxide synthase colocalizes with signs of lipid oxidation/peroxidation in human atherosclerotic plaques, Cardiovasc. Res. 43 (3) (1999) 744–754.
[51] A. Degterev, J. Hitomi, M. Germscheid, I.L. Ch'en, et al., Identification of RIP1 kinase as a specific cellular target of necrostatins, Nat. Chem. Biol. 4 (5) (2008) 313–321.
[52] D. Ofengeim, S. Mazzitelli, Y. Ito, J.P. DeWitt, et al., RIPK1 mediates a disease-associated microglial response in Alzheimer's disease, Proc. Natl. Acad. Sci. U. S. A. 114 (41) (2017) E8788–e8797.
[53] H. Liu, X. Deng, L. Zhang, C. Hongwei, et al., Knockdown RIP-1 inhibits production of oxLDL-induced inflammatory cytokines and promotes ABCA1 expression in macrophages, Int. J. Clin. Exp. Med. 11 (6) (2018) 5743–5749.
[54] D. Karunakaran, M.A. Nguyen, M. Geoffrion, D. Vreeken, et al., RIPK1 expression associates with inflammation in early atherosclerosis in humans and can be therapeutically silenced to reduce NF-κB activation and atherogenesis in mice, Circulation 143 (2) (2021) 163–177.